FULL PAPER

Electronic Structure and Chain-Length Effects in Diplatinum Polyynediyl Complexes *trans,trans*-[(X)(R₃P)₂Pt(C≡C)ₙPt(PR₃)₂(X)]: A Computational Investigation

Fedor Zhuravlev and John A. Gladysz*[a]

Abstract: Structure and bonding in the title complexes are studied using model compounds *trans,trans*-[(C₆H₅)(H₃P)₂-Pt(C≡C)ₙPt(PH₃)₂(C₆H₅)] (**PtCₓPt**; $x = 2n = 4$–26) at the B3LYP/LACVP* level of density functional theory. Conformations in which the platinum square planes are parallel are very slightly more stable than those in which they are perpendicular ($\Delta E = 0.12$ kcal mol⁻¹ for **PtC₈Pt**). As the carbon-chain length increases, progressively longer C≡C triple bonds and shorter ≡C−C≡ single bonds are found. Whereas the triple bonds in **HCₓH** become longer (and the single bonds shorter) as the interior of the chain is approached, the Pt*C*≡*C* triple bonds in **PtCₓPt** are longer than the neighboring triple bond. Also, the Pt−C bonds are shorter at longer chain lengths, but not the H−C bonds. Accordingly, natural bond orbital charge distributions show that the platinum atoms become more positively charged, and the carbon chain more negatively charged, as the chain is lengthened. Furthermore, the negative charge is localized at the two terminal C≡C atoms, elongating this triple bond. Charge decomposition analyses show no significant d–π* backbonding. The HOMOs of **PtCₓPt** can be viewed as antibonding combinations of the highest occupied π orbital of the sp-carbon chain and filled in-plane platinum d orbitals. The platinum character is roughly proportional to the Pt/Cₓ/Pt composition (e.g., $x = 4$, 31%; $x = 20$, 6%). The HOMO and LUMO energies monotonically decrease with chain length, the latter somewhat more rapidly so that the HOMO–LUMO gap also decreases. In contrast, the HOMO energies of **HCₓH** increase with chain length; the origin of this dichotomy is analyzed. The electronic spectra of **PtC₄Pt** to **PtC₁₀Pt** are simulated. These consist of two π–π* bands that redshift with increasing chain length and are closely paralleled by real systems. A finite HOMO–LUMO gap is predicted for **PtC∞Pt**. The structures of **PtCₓPt** are not strictly linear (average bond angles 179.7°–178.8°), and the carbon chains give low-frequency fundamental vibrations ($x = 4$, 146 cm⁻¹; $x = 26$, 4 cm⁻¹). When the bond angles in **PtC₁₂Pt** are constrained to 174° in a bow conformation, similar to a crystal structure, the energy increase is only 2 kcal mol⁻¹. The above conclusions should extrapolate to (C≡C)ₙ systems with other metal endgroups.

Keywords: density functional calculations · electronic structure · natural bond orbital analyses · platinum · polyynes

Introduction

There has been extensive interest recently in the synthesis and study of compounds comprised of long sp-carbon chains and transition-metal endgroups, LᵧMCₓMLᵧ.[1–14] These efforts have been motivated by a number of fundamental and applied objectives. For example, metal fragments provide dramatic stability enhancements over hydrogen or *n*-alkyl endgroups, facilitating characterization of basic properties. At longer chain lengths, models for the polymeric sp-carbon allotrope "carbyne",[15] the one-dimensional counterpart of graphite and diamond, are realized. Complexes in which metals are bridged by unsaturated ligands also exhibit a rich variety of redox and charge or energy transfer phenomena, and are under active investigation as components in molecular-scale devices.[16]

With the present state of synthetic art, LᵧMC₈MLᵧ complexes can be viewed as the boundary between short- and long-chained species.[2–14] As more and more complexes with longer chains have become available,[7,8,10–14] all of which to date are even carbon-chain polyynes or polyynediyl complexes M(C≡C)ₙM, a variety of questions have arisen or

[a] Dr. F. Zhuravlev, Prof. Dr. J. A. Gladysz
Institut für Organische Chemie
Friedrich-Alexander-Universität Erlangen-Nürnberg
Henkestraße 42, 91054 Erlangen (Germany)
Fax: (+49) 9131-852-6865
E-mail: gladysz@organik.uni-erlangen.de

been brought into sharper focus. There are numerous fundamental issues involving bond lengths and angles, not only with respect to carbyne but also the parent polyynes $H(C\equiv C)_nH$ ($\mathbf{HC_xH}$; $x=2n$). For example, how do the metal endgroups affect or regulate charge distribution, and is metal/ligand d–π communication involved? Some of these subjects have been touched upon in previous experimental and computational[17] investigations of monometallic alkynyl or polyynyl ($(C\equiv C)_nR$) complexes. Several computational studies of the polyynes $\mathbf{HC_xH}$ have been reported,[18–21] and provide important reference data for the results below.

In a recent review, we analyzed all crystallographically characterized octatetraynes and higher polyynes.[22] Many of these are diplatinum complexes of the formula *trans,trans*-$[(X)(R_3P)_2Pt(C\equiv C)_nPt(PR_3)_2(X)]$, which constitute the most extensively developed type of long-chain $L_yMC_xML_y$ species. Complexes with C_{16} bridges ($n=8$) have been isolated, and higher homologues will be reported soon.[10b] In this paper, we describe a detailed computational investigation of model compounds of the formula *trans,trans*-$[(C_6H_5)(H_3P)_2Pt(C\equiv C)_nPt(PH_3)_2(C_6H_5)]$ ($\mathbf{PtC_xPt}$, Figure 1 below), with x ($2n$) ranging from 4 to 26. Objectives include the development of 1) a comprehensive model for structure and bonding, 2) rationales for the "chain-length effects" noted for various structural, spectroscopic, and chemical properties, 3) models for the principal electronic transitions, and 4) energy profiles for endgroup rotation and carbon-chain bending—phenomena relevant to several unexpected crystallographic observations.

Other computational studies of structure and bonding in complexes of the type $L_yMC_xML_y$ have been reported.[3b,23–28] However, only one has involved species with comparable carbon-chain lengths,[28] and none have examined conformational distortions. While our data were being readied for publication, an important complementary treatment of electronic transitions in the digold complexes $[(R_3P)Au(C\equiv C)_nAu(PR_3)]$ ($n=1$–6) appeared.[25] A theoretical investigation of the electronic structure of a polymeric PtC_6Pt species, *trans,trans*-$[(H_3P)_2Pt\{(C\equiv C)_3Pt(PH_3)_2-\}_\infty]$, has also been described.[29]

Computational Methods

All calculations were carried out using density functional theory (DFT) as implemented in the Jaguar 5[30] and the Gaussian 98[31] suite of programs. Geometries were optimized using Jaguar at the B3LYP[32]/LACVP* level, which employs the Hay/Wadt[33] relativistic effective core potential with explicit treatment of the platinum valence electrons (5s,5p,5d,6s,6p) and a standard 6-31G* basis set for other atoms. Optimizations began with C_{sp}-C_{sp}-C_{sp} bond angles of 180°, and were constrained to C_{2v} symmetry for $\mathbf{PtC_xPt}$ and $D_{\infty h}$ symmetry for $\mathbf{HC_xH}$. Atoms were labeled as exemplified in Figure 1. The optimized structures were characterized as energy minima by vibrational frequency calculations at the B3LYP/LACVP* level. Total energies and zero point energies are given in Table s1 (see the Supporting Information). Natural bond orbital analyses (NBO)[34] were performed on Jaguar B3LYP/LACVP* Kohn–Sham wave functions. These were also used for the frontier molecular orbital (FMO) and charge decomposition analyses (CDA).[35] The latter were carried out with the program AOMix-CDA.[36] The lowest excited states of the Jaguar-optimized structures were calculated using time-dependent DFT at the LANL2DZ(d) level as implemented in the Gaussian 98 package.

Results and Discussion

Structures of complexes $\mathbf{PtC_xPt}$: The bond lengths calculated for $\mathbf{PtC_xPt}$ are summarized in Table 1. These and all other geometrical features are in good agreement with those found crystallographically for analogues with $(p\text{-tol})(Ar_3P)_2$-Pt endgroups ($x=6, 8, 12$).[10] The experimental data are given in italics (Table 1). The average deviation between theory and experiment is 0.019 Å, with the largest discrepancy being 0.04 Å. This close correspondence provides confidence that the computational methods accurately describe the real systems.

A representative structure is shown in Figure 1. The bond angles about the square-planar platinum atoms are very close to 90° and 180°, and those of the Pt-C_{sp}-C_{sp} and C_{sp}-C_{sp}-C_{sp} segments are very close to 180°; these data are provided in the Supporting Information (Table s2). However, it is important to note that most of the Pt-C_{sp}-C_{sp} and C_{sp}-C_{sp}-C_{sp} angles are in fact slightly less than 180° (range: 178.2–180.0°). This is further analyzed below.

Another key structural feature is the torsional relationship between the platinum square planes. Given that the geometries were optimized with C_{2v} symmetry, the relative angles are constrained to 0°. Hence, another series of calculations was conducted with $\mathbf{PtC_8Pt}$ to define the torsional-energy profile. The geometry of each additional structure was fully optimized except for the torsion-angle constraint. As shown in Figure 2, the potential surface is quite flat. Although 0° represents the energy minimum, the maximum (90°; C_2) lies only 0.12 kcal mol^{-1} higher.

One conclusion immediately follows. The crystal structures of seven complexes of the formula *trans,trans*-$[(X)(Ar_3P)_2Pt(C\equiv C)_nPt(PAr_3)_2(X)]$ with $n\geq4$, or analogues with trialkyl or aryl/alkyl phosphines, have been reported.[22] In unpublished work, we have structurally characterized several additional examples. In all cases, the torsion angles of the platinum square planes are between 0.0° and 16.6°.[37] As there is no enthalpic basis for this conformational preference, there must be a broad underlying crystal packing effect that is applicable to many lattice motifs and space groups.

Chain-length effects

Bond lengths: The computational data reveal numerous chain-length effects. The most obvious starting point involves the bond distances in Table 1. All $C\equiv C$ triple bonds lengthen and all $\equiv C-C\equiv$ single bonds contract as the sp chain in $\mathbf{PtC_xPt}$ is expanded from 4 to 26 carbon atoms (horizontal relationships). The terminal Pt–C1 single bonds also become progressively shorter (2.039 to 2.031 Å, 0.4%). The $\equiv C-C\equiv$ bonds between C2/C3 and C4/C5 exhibit the largest overall changes, −0.02 and −0.01 Å; other differences are less than ±0.008 Å. It is clear that the $C\equiv C$ and $\equiv C-C\equiv$ bond lengths are approaching distinct asymptotic limits, as opposed to a common asymptotic limit.

One apparent question is how these and other trends compare to the parent compounds $\mathbf{HC_xH}$. The computational data show similar patterns,[18–21,38] but with two notable ex-

Table 1. Bond lengths in *trans,trans*-[(Ar)(R$_3$P)$_2$Pt(C≡C)$_n$Pt(PR$_3$)$_2$(Ar)]: Calculated (Ar/PR$_3$ = Ph/PH$_3$; **PtC$_x$Pt**) and *Experimental* (Ar/PR$_3$/n = *p*-tol/P(*p*-tol)$_3$/3, *p*-tol/PPh$_3$/4, *p*-tol/P(*p*-tol)$_3$/5, *p*-tol/P(*p*-tol)$_3$/6) values (unitalicized/*italicized*).

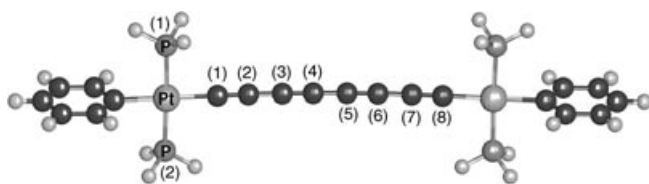| | Number of sp-carbon atoms (x) in **PtC$_x$Pt** | | | | | | | | | | |
	4	6	8	10	12	14	16	18	20	24	26
Pt–C1	2.039	2.035	2.035	2.034	2.033	2.032	2.031	2.032	2.031	2.031	2.031
		2.030(3)	*2.011(4)*	*1.990(3)*	*1.990(3)*						
C1–C2	1.233	1.235	1.237	1.238	1.237	1.238	1.238	1.239	1.239	1.238	1.239
		1.193(5)	*1.218(6)*	*1.190(5)*	*1.233(4)*						
C2–C3	1.366	1.355	1.353	1.349	1.350	1.348	1.347	1.347	1.346	1.345	1.345
		1.388(5)	*1.368(6)*	*1.404(4)*	*1.358(4)*						
C3–C4		1.231	1.233	1.234	1.235	1.235	1.236	1.236	1.236	1.236	1.237
		1.211(7)	*1.223(6)*	*1.215(5)*	*1.210(5)*						
C4–C5			1.346	1.342	1.339	1.337	1.337	1.336	1.337	1.335	1.335
			1.367(9)	*1.342(5)*	*1.356(5)*						
C5–C6				1.236	1.237	1.238	1.238	1.239	1.239	1.239	1.240
				1.228(7)	*1.211(5)*						
C6–C7					1.338	1.336	1.335	1.333	1.333	1.332	1.332
					1.344(7)						
C7–C8						1.238	1.239	1.240	1.240	1.241	1.241
C8–C9							1.334	1.333	1.332	1.331	1.330
C9–C10								1.240	1.240	1.242	1.242
C10–C11									1.332	1.330	1.330
C11–C12										1.242	1.241
C12–C13											1.330
Pt–C(Aryl)	2.103	2.101	2.100	2.100	2.099	2.099	2.099	2.098	2.098	2.098	2.098
		2.056(5)	*2.064(4)*	*2.078(3)*	*2.099(3)*						
Pt–P1	2.291	2.293	2.296	2.296	2.297	2.297	2.298	2.299	2.299	2.300	2.300
		2.295(10)	*2.307(11)*	*2.301(8)*	*2.297(8)*						
Pt–P2	2.299	2.300	2.303	2.305	2.306	2.306	2.307	2.307	2.307	2.308	2.308
		2.300(10)	*2.300(11)*	*2.310(9)*	*2.306(8)*						

Figure 1. Representative computed structure (**PtC$_8$Pt**) and atom-labeling scheme.
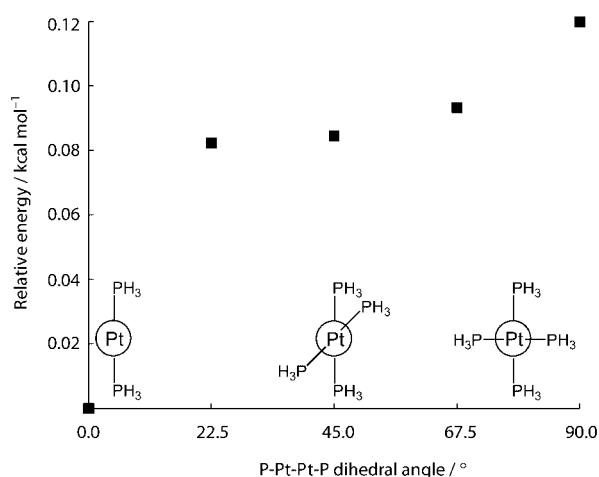

Figure 2. Energy profile for endgroup rotation in **PtC$_8$Pt**.

ceptions: 1) the terminal H–C single bond lengths remain essentially constant (1.066 Å); 2) the C≡C triple bonds are shortest at the termini (C1/C2 1.213 Å in **HC$_4$H** or 1.218 Å in **HC$_{20}$H**), and become progressively longer as the midpoint of the chain is approached. In contrast, the C1/C2 triple bonds in **PtC$_x$Pt** are always longer than the neighboring C3/C4 triple bonds; subsequent interior triple bonds (e.g., C5/C6) become, as with **HC$_x$H**, progressively longer (vertical relationships in Table 1). Although analogous trends are seen in some experimental data, the estimated standard deviation (esd) values are normally too large to permit rigorous conclusions.[39] In any case, our data suggest an overriding endgroup effect on the C1/C2 distances in **PtC$_x$Pt**, a subject addressed in detail below.

For both **PtC$_x$Pt** and **HC$_x$H**, the ≡C–C≡ single bonds become progressively shorter as the midpoint of the chain is approached. However, single/triple bond alternation is clearly maintained in each molecule, in accord with all previous computational studies of X(C≡C)$_n$X systems.[17d,18,19,21] The difference in length between the shortest ≡C–C≡ single bond and the longest C≡C triple bond has been defined as the bond-alternation parameter, δ.[40] The value for **PtC$_{20}$Pt** (0.097 Å) is smaller than that of **HC$_{20}$H** (0.105 Å), and that for **PtC$_{26}$Pt** (0.094 Å) is smaller than those of **HC$_{26}$H** (1.102 Å) and **HC$_{40}$H** (0.097 Å; the longest such species computationally investigated).[21b,38] This suggests that **PtC$_x$Pt** has a lower degree of bond alternation than **HC$_x$H**, and converges to an asymptotic limit more rapidly. The anionic species **HC$_x$**$^-$ exhibits a still lower degree of bond alternation,[21a,c] implying a correlation with the electronegativity of the endgroup.

In order to interpret the different bond-length patterns involving the HC≡C and PtC≡C linkages in **HC$_x$H** and

PtC_xPt, the nature of interactions of the platinum endgroups with the sp-carbon chains must be analyzed. To what degree is there communication through the π manifold and how important are the other contributions, such as charge effects? In previous computational studies of metal–alkynyl complexes, it has been noted that the MC≡C bond lengths are strong functions of the metal–carbon σ component and the "tightness" of a C≡C triple bond.[17b] We therefore turned to population analysis as a means to separate the σ- and π-bonding contributions.

Population and charge distribution analysis: Natural bond orbital (NBO) analysis has proved to be a powerful tool for describing bonding and charge distribution in terms of localized orbitals.[41] Table 2 lists the natural electron populations and corresponding cumulative bond orders calculated for **PtC_xPt**; the latter were taken as half the difference of the bonding and antibonding electron populations.

The cumulative C≡C triple bond orders (Table 2) generally show an inverse relationship to the bond lengths (Table 1), except for the terminal PtC≡C moieties. These have the highest bond order of all triple bonds but remain longer than the C3/C4 triple bonds. Upon going from **PtC_4Pt** to **$PtC_{26}Pt$**, the PtC≡C bond orders drop from 2.782 to 2.727 (2.00%), in accord with the bond-length trend noted above. Inspection of the natural populations shows that this decrease is due to electron depletion in the π bonding orbitals and increased occupancy of the π* antibonding orbitals. There is virtually no change in the σ bond order (0.983 to 0.982, 0.1%).

The change in the π populations of the C3/C4 C≡C triple bond is even more pronounced. Now the cumulative bond orders decrease from 2.664 to 2.600 (2.4%), again with no change in the σ population. Indeed, all C≡C bonds undergo bond-order reduction through the π manifold, although comparisons must be made over narrower ranges (e.g., from **$PtC_{10}Pt$** to **$PtC_{26}Pt$** for C5/C6 C≡C). In contrast, the C2/C3 ≡C−C≡ single bond order shows a gradual increase from 0.967 to 0.973 (0.62%).

Thus, while the NBO population analysis describes quite satisfactorily the changes in the internal bond lengths (C2/C3 through C(x−2)/C(x−3)), it cannot adequately account for all features of the PtC≡C linkage. One factor often invoked to rationalize metal–carbon bond-length trends is d–π* backbonding. If d–π* backbonding is significant, a corresponding increase in the π* population of the PtC≡C bond would be expected. As it turns out, this population is small (only 0.11 e) and remains the smallest population of all π* orbitals across the entire **PtC_xPt** series. Moreover, this trend exactly parallels that observed for **HC_xH**, for which no backbonding is possible. Additional probes for d–π* interactions will be described below.

Table 3 lists the NBO charge distributions calculated for **PtC_xPt**. These provide complimentary insight regarding the PtC≡C bond lengths. Upon going from **PtC_4Pt** to **$PtC_{26}Pt$**, the platinum atoms become more positively charged, whereas the sp-carbon chains become more negatively charged (bottom entry). This is consistent with the bond-length trend as well as the experimental Brønsted acidities of terminal

polyynes.[42] The latter increase with sp-carbon-chain length, indicating progressively greater negative charge stabilization.

We also find, in agreement with earlier computational studies of metal polyynyl complexes,[17d] substantial localization of the negative charge on the two terminal C≡C atoms at each end. This is particularly pronounced with shorter carbon chains. For example, 89% of the total charge on the chain in **PtC_8Pt** is found at C1/C2. As the chain lengthens, some negative charge flows towards the midpoint. Thus, 77% of the total charge on the chain in **$PtC_{26}Pt$** is found at C1/C2. Charge alternation patterns also develop. Once **$PtC_{10}Pt$** is reached, the negatively charged C1/C2 atoms are followed by a positively charged C3 atom. However, regardless of the sign, the total charge on the interior atoms (C3 to C(x−3)) is always much less than those on C1/C2.

The charge distributions provide a clear rationale for the endgroup effect upon bond lengths: The increase in Pt/C1 charge polarizations with chain length leads to stronger electrostatic attraction between the platinum atoms and the carbon chains and shorter bonds, while repulsion between the negatively charged C1 and C2 atoms causes the "anomalous" lengthening of the C1/C2 C≡C bond relative to interior C≡C bonds. Also, the electrostatic attraction between C2 and C3 increases with chain length, consistent with the greater decrease in bond lengths as compared to other ≡C−C≡ bonds.

This model also rationalizes an analogous endgroup effect found in a computational study of **LiC_xLi** (x=2–8).[44] For x=6 and 8, the terminal LiC≡C triple bonds were similarly longer than the neighboring internal C≡C bonds. We therefore predict that comparable trends will be found for all conjugated polyynes with electropositive endgroups.

Orbital analyses: Frontier molecular orbital (FMO) analysis is another valuable approach to rationalizing molecular properties.[45] Accordingly, the FMOs of **PtC_4Pt** to **$PtC_{26}Pt$** were calculated. The contours and energies of the HOMOs through to **$PtC_{20}Pt$** are summarized in Table 4, together with the degree of platinum/sp-carbon-chain character.

The HOMOs can be viewed as antibonding combinations of the highest occupied π orbital of the sp-carbon-chain fragment and the filled in-plane d orbitals of the two platinum fragments. The nodal patterns on the carbon chains are analogous to those that would be expected for simple polyynes and polyenes from the Hückel MO theory. The next highest occupied orbitals (HOMO−1) are essentially out-of-plane counterparts of the HOMOs that utilize orthogonal platinum d and C≡C π orbitals. The LUMOs are bonding combinations of the lowest unoccupied π orbital of the carbon-chain fragment and the platinum d orbitals.

The HOMOs are strongly delocalized over the Pt/C_x/Pt framework, with the platinum character roughly proportional to the Pt/C_x/Pt composition. This is significant for the first members of the series (31% in **PtC_4Pt**, for which 33% of the atoms are platinum), but drops sharply for later members of the series (6% in **$PtC_{20}Pt$**, for which 9% of the atoms are platinum). Consequently, the HOMOs of the longer-chain compounds are almost exclusively carbon-

Table 2. Natural population and bond order data for **PtC$_x$Pt**.[a,b]

	Number of sp-carbon atoms (x) in **PtC$_x$Pt**										
	4	6	8	10	12	14	16	18	20	24	26
Pt-total	77.774	77.770	77.770	77.768	77.767	77.766	77.766	77.766	77.765	77.765	77.765
π^1 C1-C2	1.914	1.894	1.883	1.876	1.871	1.867	1.865	1.862	1.861	1.858	1.857
π^1 C1-C2*	0.108	0.113	0.114	0.113	0.113	0.113	0.113	0.113	0.113	0.112	0.112
π^2 C1-C2	1.900	1.886	1.877	1.871	1.867	1.864	1.861	1.859	1.858	1.855	1.854
π^2 C1-C2*	0.106	0.112	0.112	0.112	0.112	0.111	0.111	0.111	0.110	0.110	0.110
σ C1-C2	1.982	1.982	1.982	1.982	1.982	1.982	1.982	1.982	1.982	1.982	1.982
σ C1-C2*	0.017	0.018	0.018	0.018	0.018	0.018	0.018	0.018	0.018	0.018	0.018
bond order	2.782	2.760	2.749	2.743	2.738	2.735	2.733	2.731	2.729	2.727	2.727
σ C2-C3	1.970	1.973	1.973	1.973	1.973	1.973	1.973	1.973	1.973	1.973	1.974
σ C2-C3*	0.036	0.029	0.029	0.029	0.028	0.028	0.028	0.028	0.028	0.028	0.028
bond order	0.967	0.972	0.972	0.972	0.972	0.972	0.972	0.973	0.973	0.973	0.973
π^1 C3-C4		1.866	1.848	1.838	1.832	1.828	1.825	1.823	1.821	1.818	1.817
π^1 C3-C4*		0.172	0.184	0.188	0.190	0.191	0.192	0.192	0.192	0.193	0.193
π^2 C3-C4		1.851	1.839	1.831	1.826	1.822	1.820	1.818	1.816	1.814	1.813
π^2 C3-C4*		0.173	0.185	0.189	0.191	0.192	0.193	0.193	0.194	0.194	0.194
σ C3-C4		1.976	1.976	1.976	1.976	1.976	1.976	1.976	1.976	1.976	1.976
σ C3-C4*		0.021	0.021	0.021	0.021	0.020	0.020	0.020	0.020	0.020	0.020
bond order		2.664	2.637	2.624	2.616	2.611	2.608	2.605	2.603	2.600	2.600
σ C4-C5		1.975	1.975	1.975	1.975	1.975	1.975	1.975	1.975	1.975	1.975
σ C4-C5*		0.022	0.022	0.022	0.022	0.022	0.022	0.022	0.022	0.022	0.022
bond order		0.976	0.976	0.976	0.977	0.977	0.977	0.977	0.977	0.977	0.977
π^1 C5-C6			1.831	1.821	1.820	1.812	1.809	1.807	1.804	1.808	
π^1 C5-C6*			0.198	0.202	0.213	0.205	0.207	0.208	0.209	0.215	
π^2 C5-C6			1.826	1.817	1.817	1.810	1.807	1.805	1.802	1.806	
π^2 C5-C6*			0.198	0.203	0.213	0.205	0.207	0.208	0.209	0.216	
σ C5-C6			1.976	1.976	1.976	1.976	1.976	1.976	1.976	1.976	
σ C5-C6*			0.021	0.021	0.021	0.021	0.021	0.021	0.021	0.021	
bond order			2.608	2.595	2.583	2.584	2.578	2.576	2.572	2.569	
σ C6-C7				1.975	1.972	1.975	1.976	1.976	1.976	1.973	
σ C6-C7*				0.022	0.020	0.022	0.022	0.022	0.022	0.020	
bond order				0.977	0.976	0.976	0.977	0.977	0.977	0.976	
π^1 C7-C8					1.789	1.810	1.807	1.801	1.797	1.788	
π^1 C7-C8*					0.200	0.206	0.220	0.211	0.214	0.207	
π^2 C7-C8					1.786	1.808	1.806	1.800	1.796	1.787	
π^2 C7-C8*					0.200	0.206	0.220	0.211	0.214	0.207	
σ C7-C8					1.966	1.974	1.976	1.976	1.976	1.973	
σ C7-C8*					0.016	0.019	0.021	0.021	0.020	0.018	
bond order					2.563	2.580	2.564	2.567	2.561	2.558	
σ C8-C9						1.965	1.973	1.975	1.976	1.975	
σ C8-C9*						0.017	0.020	0.022	0.021	0.022	
bond order						0.974	0.976	0.977	0.977	0.977	
π^1 C9-C10						1.777	1.801	1.795	1.793		
π^1 C9-C10*						0.205	0.209	0.214	0.214		
π^2 C9-C10						1.776	1.800	1.794	1.792		
π^2 C9-C10*						0.205	0.209	0.214	0.214		
σ C9-C10						1.966	1.974	1.976	1.976		
σ C9-C10*						0.016	0.019	0.021	0.021		
bond order						2.546	2.569	2.558	2.556		
σ C10-C11							1.966	1.976	1.976		
σ C10-C11*							0.017	0.022	0.021		
bond order							0.974	0.977	0.977		
π^1 C11-C12								1.796	1.796		
π^1 C11-C12*								0.212	0.225		
π^2 C11-C12								1.796	1.795		
π^2 C11-C12*								0.211	0.225		
σ C11-C12								1.974	1.976		

Table 2. (Continued)

	Number of sp-carbon atoms (x) in $\textbf{PtC}_x\textbf{Pt}$										
	4	6	8	10	12	14	16	18	20	24	26
σ C11-C12*										0.019	0.021
bond order										2.562	2.548
σ C12-C13										1.966	1.973
σ C12-C13*										0.017	0.020
bond order										0.975	0.976
π¹ C13-C14											1.767
π¹ C13-C14*											0.209
π² C13-C14											1.766
π² C13-C14*											0.209
σ C13-C14											1.967
σ C13-C14*											0.016
bond order											2.532

[a] Bond orders are calculated as half the difference of the bonding and antibonding electron population as determined by NBO analysis. [b] Unstarred: bonding natural orbitals; starred: antibonding natural orbitals.

Table 3. Natural charge in $\textbf{PtC}_x\textbf{Pt}$.

	Number of sp-carbon atoms (x) in $\textbf{PtC}_x\textbf{Pt}$										
	4	6	8	10	12	14	16	18	20	24	26
Pt	0.226	0.230	0.230	0.232	0.233	0.234	0.234	0.234	0.235	0.235	0.235
C1	−0.354	−0.316	−0.296	−0.280	−0.269	−0.261	−0.256	−0.251	−0.247	−0.240	−0.239
C2	−0.182	−0.209	−0.215	−0.220	−0.225	−0.227	−0.228	−0.230	−0.231	−0.234	−0.233
C3		−0.033	−0.002	0.015	0.026	0.033	0.039	0.044	0.047	0.054	0.055
C4			−0.060	−0.067	−0.071	−0.073	−0.076	−0.077	−0.078	−0.080	−0.080
C5				−0.030	−0.014	−0.002	0.003	0.008	0.012	0.019	0.025
C6					−0.038	−0.101	−0.042	−0.047	−0.048	−0.051	−0.105
C7						0.037	−0.092	−0.004	−0.001	0.006	0.127
C8						0.052	−0.090	−0.029	−0.035	−0.106
C9							0.042	−0.090	−0.002	0.004
C10								0.059	−0.022	−0.026
C11									−0.089	−0.003
C12									0.063	−0.080
C13										0.049
total C_x chain charge	−0.536	−0.558	−0.572	−0.582	−0.590	−0.596	−0.600	−0.604	−0.607	−0.611	−0.613

chain-based. The HOMO−1 orbitals and LUMOs exhibit parallel trends.

As shown in Figure 3, both the HOMO and LUMO energies monotonically decrease upon going from $\textbf{PtC}_4\textbf{Pt}$ to $\textbf{PtC}_{26}\textbf{Pt}$. The former trend is in sharp contrast to that of $\textbf{HC}_x\textbf{H}$ (inset). For the hydrocarbons, the HOMO energies monotonically increase with chain length.[38] The basis for this rise is the number of nodes per C≡C unit, which increases from 1/2 for $\textbf{HC}_4\textbf{H}$ to 1 for $\textbf{HC}_\infty\textbf{H}$. For reference, note that the increase in HOMO energies upon going from $\textbf{HC}_4\textbf{H}$ to $\textbf{HC}_{20}\textbf{H}$ (+1.06 eV) is more pronounced than the decrease upon going from $\textbf{PtC}_4\textbf{Pt}$ to $\textbf{PtC}_{20}\textbf{Pt}$ (−0.33 eV). The decrease in LUMO energies in both series of compounds is substantial ($\textbf{HC}_4\textbf{H}$ to $\textbf{HC}_{20}\textbf{H}$, −2.77 eV; $\textbf{PtC}_4\textbf{Pt}$ to $\textbf{PtC}_{20}\textbf{Pt}$, −1.64 eV).

The effect of the platinum endgroup upon the HOMO energies of $\textbf{PtC}_x\textbf{Pt}$ can be rationalized as follows. As noted above, the HOMOs are antibonding combinations of the highest occupied π orbital of the carbon-chain fragment and occupied d orbitals on the platinum fragments. This destabi-

lizing interaction, which has no counterpart in $\textbf{HC}_x\textbf{H}$, is reflected in the consistently higher HOMO energies (e.g., −4.69 eV for $\textbf{PtC}_8\textbf{Pt}$ versus −6.44 eV for $\textbf{HC}_8\textbf{H}$). Since the platinum and C_1 coefficients decrease with chain length, the destabilization attenuates. This diminution in energy is apparently larger than the increase associated with the greater number of nodes in the carbon-chain fragment.[46] This trend has been documented computationally for other $M(C≡C)_nM$ systems, although over a smaller range of chain lengths ($n ≤ 4$), and similarly interpreted.[3b, 23c]

Importantly, the LUMO energies of $\textbf{PtC}_x\textbf{Pt}$ decrease more rapidly than the HOMO energies. Consequently, the HOMO–LUMO gap also decreases, but in progressively smaller increments suggestive of a non-zero value for the infinite chain limit $\textbf{PtC}_\infty\textbf{Pt}$. To probe this point, the HOMO–LUMO gap was plotted versus $1/n$, the inverse of the number of C≡C bonds ($1/2x$). As illustrated in Figure s1 (see Supporting Information), the relationship was linear ($r^2 = 0.995$). The y intercept, corresponding to $n = \infty$, indicated a residual value of 1.49 eV (832 nm). Optical spectra of

Table 4. Selected data for the HOMOs of **PtC$_x$Pt**.

	Energy [eV]	Symmetry	Pt/sp-chain character [%]	HOMO[a]
PtC$_4$Pt	−4.656	a$_2$	31/66	
PtC$_6$Pt	−4.663	b$_1$	22/76	
PtC$_8$Pt	−4.696	a$_2$	17/82	
PtC$_{10}$Pt	−4.749	b$_1$	14/86	
PtC$_{12}$Pt	−4.801	a$_2$	10/90	
PtC$_{14}$Pt	−4.852	b$_1$	10/90	
PtC$_{16}$Pt	−4.898	a$_2$	8/92	
PtC$_{18}$Pt	−4.942	b$_1$	7/93	
PtC$_{20}$Pt	−4.983	a$_2$	6/94	

[a] The relative sizes of the orbitals reflect the coefficients at the corresponding atoms.
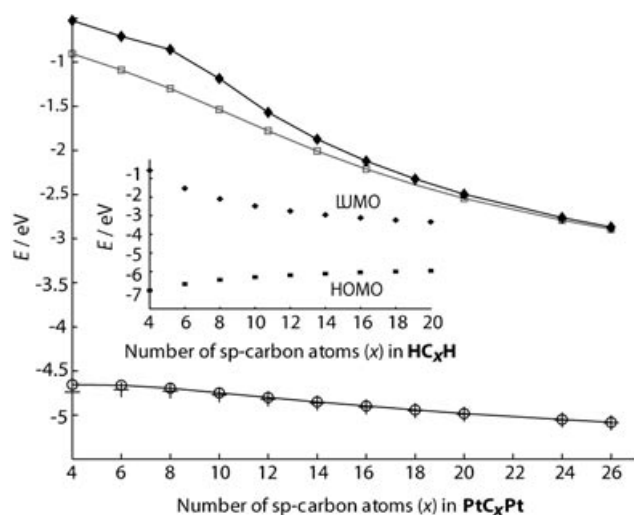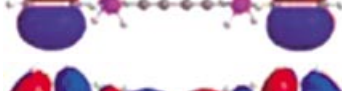
Figure 3. Energies of frontier molecular orbitals (FMOs) of **PtC$_x$Pt** as a function of chain length in which ○ = HOMO, + = HOMO−1, □ = LUMO, and ◆ = LUMO+1, and (inset) related data for **HC$_x$H**.

all long-chain conjugated polyynes studied to date lead to analogous conclusions,[8,11,47] as further elaborated below.

These FMO properties have some important ramifications. First, on the basis of Koopmans' theorem, an increase in ionization potential with chain length would be expected. Accordingly, cyclic voltammograms of the diplatinum complexes *trans,trans*-[(X)(R$_3$P)$_2$Pt(C≡C)$_n$Pt(PR$_3$)$_2$(X)],[10–12] as well as related dirhenium species,[8,9] indicate thermodynamically less favorable oxidations with increasing chain length.[48] Secondly, other combinations of occupied and unoccupied orbitals mirror the decreasing HOMO–LUMO gap, as illustrated for the LUMO+1 and HOMO−1 energies in Table 5. This should lead to progressively redshifted UV/visible absorptions, as observed with all families of conjugated polyynes. The HOMO and HOMO−1 energies are nearly degenerate, with a vanishing small difference at longer sp-chain lengths where the chain character becomes very high.

One caveat regarding the ionization potentials deserves emphasis. The above data were obtained using DFT calculations, and Kohn–Sham orbitals were used for the FMO analyses. It is still not clear to what degree Kohn–Sham orbitals can be reliably used in connection with the Koopmans' theorem. However, the recent literature indicates that Kohn–Sham orbitals can be used with confidence at least qualitatively.[49] Furthermore, a linear relationship between Har-

Table 5. Charge decomposition analysis of **PtC₄Pt**, with **D** = **PtC₄⁻** (donor) and **A** = **Pt⁺** (acceptor).[a]

Orbital	Energy [eV]	Symmetry	d (**D**→**A**)	b (**A**→**D**)	r	Orbital
HOMO-10	−6.91	b_2	0.124	−0.012	−0.154	
HOMO-9	−6.84	a_1	0.11	−0.014	−0.118	
HOMO-8	−6.72	b_1	0.006	0.018	−0.066	
HOMO-7	−6.48	b_2	0.048	−0.02	−0.128	
HOMO-6	−6.47	a_1	0.066	0.012	−0.116	
HOMO-5	−6.24	a_2	0	0	0	
HOMO-4	−6.24	b_1	0	0	0	
HOMO-3	−5.98	b_2	0	0	0.002	
HOMO-2	−5.91	a_1	0	0.002	−0.004	
HOMO-1	−4.74	b_2	0.022	−0.022	−0.126	
HOMO	−4.66	a_2	0.046	−0.014	−0.094	
total over all MO			0.283	−0.084	−0.521	

[a] d represents the donation from **D** to **A**, and b the back-donation from **A** to **D**; r is the electron repulsion term.

tree–Fock and Kohn–Sham orbital energies has been observed.[49]

Charge decomposition analysis: As noted above, the NBO population analysis gave no indication of any significant d–π* backbonding (Table 2). In order to further probe this point, a charge decomposition analysis (CDA)[35] was performed on the first member of the series, **PtC₄Pt**. This technique partitions ligand–metal interactions into donation/back-donation components analogous to those of the Dewar–Chatt–Duncanson model.

Towards this end, the linear combination of Kohn–Sham orbitals of the donor (**D**) fragment **PtC₄⁻** and the acceptor (**A**) fragment **Pt⁺** were used to describe **PtC₄Pt**. The results of the charge decomposition are summarized in Table 5. The

quantity d represents the donation from **D** to **A**, and b the back-donation from **A** to **D**. The electron repulsion term r indicates the amount of electron density removed from the bonding area into non-overlapping regions. These quantities can be totaled over all molecular orbitals (final entry). From the resulting absolute values of d and b, a net flow of electrons from **PtC₄⁻** to **Pt⁺** is apparent. The negative sign of r indicates a reduced closed-shell repulsion with respect to the superimposed fragments.

Additional insight can be gleaned from the relative contributions of the ten highest occupied molecular orbitals to bond formation. The four orbitals HOMO−2, HOMO−3, HOMO−4, and HOMO−5 have a high degree of phenyl character and make little or no contribution to the CDA analysis. The four orbitals with the largest d values,

HOMO−6, HOMO−7, HOMO−9, and HOMO−10, are all of local σ symmetry, indicating the importance of σ donation. The two orbitals with the next largest d values, HOMO and HOMO−1, are of local π symmetry, and contribute to electron donation through the π manifold, that is, ligand-to-metal π bonding.

In higher homologues of **PtC$_4$Pt**, the **PtC$_x^-$** moiety should be a somewhat weaker σ donor and a stronger π acceptor, in accord with the HOMO–LUMO energy trends noted above. Nonetheless, a reversal of the absolute values of d and b would not be expected. We therefore conclude that in polyynyl/Pt^{II} complexes, the polyynyl fragment acts mainly as a σ/π donor with essentially no back-donation from the metal. This is in agreement with a combined photoelectron spectroscopy/theoretical study of *trans*-[(PEt$_3$)$_2$Pt(C≡CH)$_2$], in which no evidence for π backbonding was found.[50]

Chain-length effects—electronic transitions: The diplatinum complexes *trans, trans*-[(X)(R$_3$P)$_2$Pt(C≡C)$_n$Pt(PR$_3$)$_2$(X)] exhibit richly featured electronic spectra.[10–12] As the sp-carbon chain is lengthened, progressively more intense and longer wavelength absorptions are observed. In an effort to better understand the origin of these absorptions, time-dependent DFT calculations were performed for **PtC$_4$Pt** through to **PtC$_{10}$Pt**. Figure 4 depicts the simulated absorption spectra, each of which features two bands. That with the longer wavelength is termed "band I", and the other "band II". Table 6 lists the corresponding states, energies, and oscillator strengths.

For **PtC$_4$Pt**, band I is essentially single configurational and corresponds to a HOMO–LUMO excitation. For the higher homologues, band I becomes increasingly two-configurational, but retains dominant HOMO–LUMO character. At the same time, the oscillator strengths plummet, as reflected by the diminishing peak intensities in Figure 4. In
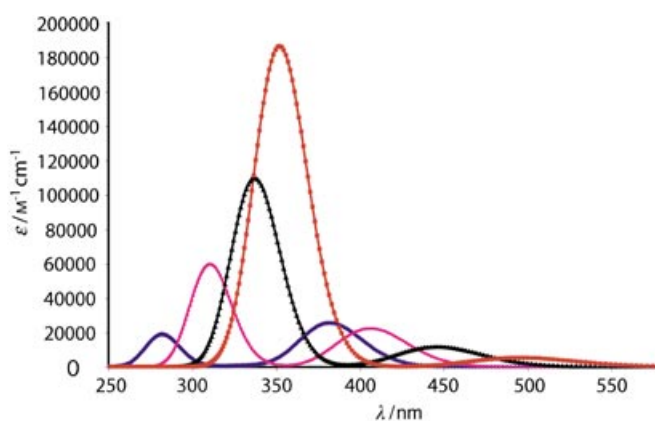

Figure 4. Simulated absorption spectra for **PtC$_x$Pt** from time-dependent DFT calculations. Color coding: blue = PtC$_4$Pt, pink = PtC$_6$Pt, black = PtC$_8$Pt, and red = PtC$_{10}$Pt.

contrast, the oscillator strengths for band II steadily increase. This absorption is multiconfigurational, but the HOMO–LUMO character gradually rises.

To gain additional insight into the nature of these transitions, the difference electron densities for the ground and excited states corresponding to bands I and II were calculated. As exemplified for **PtC$_6$Pt** in Figure 5,[51] this easily allows both absorptions to be assigned as π–π* transitions that originate in the sp-carbon chain. This even holds for **PtC$_4$Pt**, where the FMOs have more platinum character.

The simulated spectra in Figure 4 can be contrasted with those of analogous experimental systems. Data for PtC$_x$Pt complexes with (*p*-tol)(*p*-tol$_3$P)$_2$Pt endgroups are summarized in Table 7.[10] Those for complexes with (C$_6$F$_5$)(*p*-tol$_3$P)$_2$Pt and (C$_6$F$_5$)(Et$_3$P)$_2$Pt endgroups are similar.[11] These real systems contain additional chromophores, resulting in extra absorptions. When coupled with vibrational fine structure, which is often observed,[11,47a] comparisons become complicated. Nonetheless, several key features are replicated.[52]

First, the increasingly intense longest wavelength absorptions of the PtC$_{10}$Pt, PtC$_{12}$Pt, PtC$_{16}$Pt, and PtC$_{20}$Pt complexes (Table 7) clearly correspond to band II of **PtC$_x$Pt**. Second, several evenly spaced weaker longer wavelength bands are observed with all PtC$_8$Pt complexes, followed by a much stronger band at shorter wavelengths (e.g., 359, 387, and 419 nm with ε 17600–5600 M^{-1} cm^{-1}, then 337 nm with ε 102000 M^{-1} cm^{-1} as given in Table 7). The weaker absorptions likely correspond to vibrational progressions of band I, and the strongest one to band II. Methyl-capped polyynes Me(C≡C)$_n$Me are also charac

Table 6. Calculated singlet excitations for **PtC$_x$Pt** in gas phase.

|	Band	Orbitals	Contribution [%]	E [eV]	λ_{max} [nm]	Oscillator strength
PtC$_4$Pt	I	HOMO−1→LUMO+10	3	3.25	382	0.353
		HOMO→LUMO	90			
	II	HOMO−1→LUMO+4	85	4.39	282	0.258
		HOMO→LUMO+5	7			
		HOMO→LUMO+19	3			
PtC$_6$Pt	I	HOMO−1→LUMO+4	16	3.05	406	0.311
		HOMO→LUMO	81			
	II	HOMO−1→LUMO+4	46	3.99	310	0.824
		HOMO→LUMO	9			
		HOMO→LUMO+5	13			
		HOMO→LUMO+11	28			
PtC$_8$Pt	I	HOMO−1→LUMO+1	33	2.78	446	0.160
		HOMO→LUMO	67			
	II	HOMO−1→LUMO+1	30	3.68	337	1.504
		HOMO→LUMO	18			
		HOMO→LUMO+5	39			
		HOMO→LUMO+9	5			
PtC$_{10}$Pt	I	HOMO−1→LUMO+1	41	2.50	496	0.071
		HOMO→LUMO	59			
	II	HOMO−1→LUMO+1	23	3.52	352	2.569
		HOMO→LUMO	21			
		HOMO→LUMO+5	42			
		HOMO−3→LUMO+2	2			

www.chemeurj.org
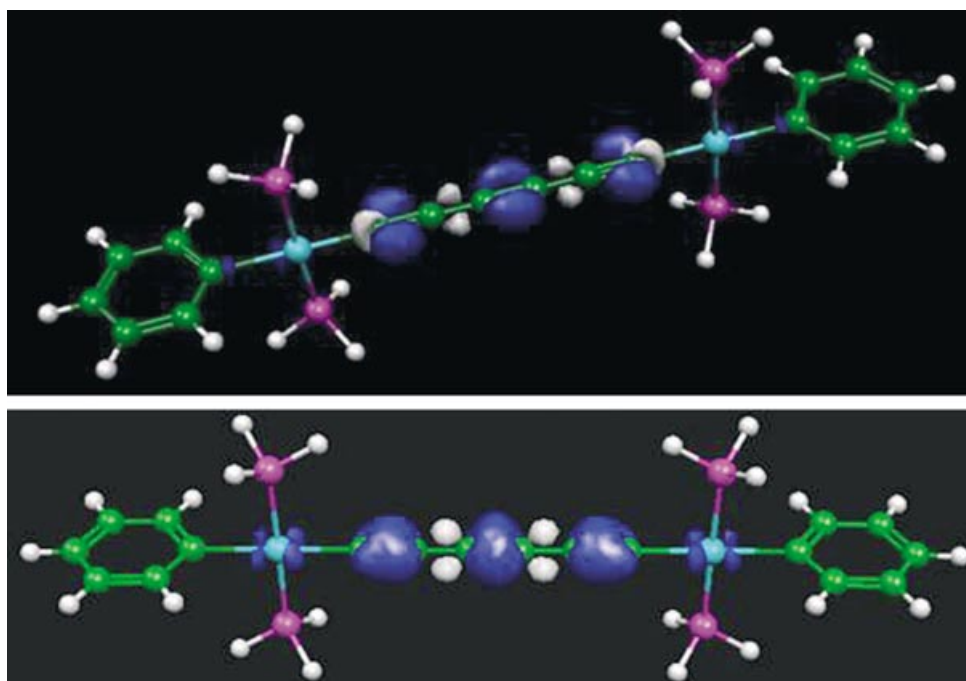
Figure 5. Change of electron density from ground to singlet excited states of **PtC₆Pt**. Top: band I; bottom: band II. Color coding: ground state blue; excited state white.

Table 7. UV-visible data for *trans,trans*-[(p-tol)(p-tol₃P)₂Pt(C≡C)ₙPt(P-p-tol₃)₂(p-tol)].[a]

Number of sp-carbon atoms ($x=2n$)	λ_{max} [nm] [ε (M⁻¹cm⁻¹)]
6	329 [33 600], 351 [25 600], 376 [8800]
8	305 [99 200], 337 [101 600], 359 [17 600], 387 [8800], 419[5600]
10	281 [74 000], 316 [110 000], 327 [118 000], 350[212 000]
12	323 [106 000], 345 [201 000], 371[361 000]
16	309 [50 400], 334 [61 600], 357 [103 000], 383 [219 000], 411[365 000]
20	296 [71 200], 312 [76 800], 328 [80 000], 347 [78 400], 413 [262 000], 446[368 000]

[a] 1.25×10^{-6} M in CH₂Cl₂.

most other X(C≡C)∞X systems (550–569 nm).[8,47] Pentafluorophenyl-substituted platinum complexes yield slightly lower limits (527–492 nm).[11] However, the most important point is that these plots experimentally confirm a persistent, non-zero band gap at infinite chain length, complementing the conclusion from Figure 3. This is in agreement with the single/triple bond alternation maintained in the longer-chain species **PtC₂₆Pt** and **HC₄₀H**, and the convergence to distinct asymptotic limits for the C≡C and ≡C−C≡ bond lengths.

terized by very weak longer wavelength absorptions that show vibrational subbands.[53] For the PtC₆Pt complex, the absorption at 329 nm most likely represents band II.[54]

In order to further evaluate these assignments, the λ_{max} values calculated for band II were plotted versus n (x/2). A linear relationship was obtained ($r^2=0.992$), as shown in Figure s2 (see the Supporting Information). The experimental absorptions from Table 7 assigned to band II were similarly plotted, and another linear relationship was obtained ($r^2=0.994$). Although a perfect match would not be expected given the structural differences and the limitations of the theory, portions of the lines are roughly coincident and the calculations extrapolate surprisingly well to the transition energies of the real systems.

For the four longest chain complexes in Table 7, the λ_{max} values for band II were plotted versus $1/n$ (Figure s2, Supporting Information). The resulting line ($r^2=0.981$) gives a y intercept of 532 nm, the extrapolated value for **PtC∞Pt**. Since endgroup effects will be negligible at infinite chain lengths, this should closely approximate that of the one-dimensional polymeric carbon allotrope carbyne. The value is in quite good agreement with those similarly predicted from

sp-Carbon-chain bending: The energy profile for torsional motion of the platinum endgroups was computed above (Figure 2). The conformation of the carbon chain represents yet another structural variable. Of the approximately fifty crystallographically characterized tetraynes and higher polyynes, nearly all exhibit distinct deviations from linearity.[22] There are only four such compounds in which the average of all X-C$_{sp}$-C$_{sp}$ and C$_{sp}$-C$_{sp}$-C$_{sp}$ bond angles is >178.8°. Both bow- and S-shaped conformations are common, and other motifs also occur. A nonlinearity parameter has been defined.[22]

Due to the C_{2v} symmetry constraint, all of the structures calculated for **PtC$_x$Pt** exhibit symmetrical bow conformations; S-shaped conformations are arbitrarily excluded. The average of all Pt-C$_{sp}$-C$_{sp}$ and C$_{sp}$-C$_{sp}$-C$_{sp}$ bond angles ranges from 179.9° (**PtC₆Pt**) to 179.2° (**PtC₁₂Pt**), as summarized in Table s2 (see the Supporting Information). These structures

show a greater degree of linearity than the real systems, as might intuitively be expected for gas-phase calculations where no crystal packing effects are possible. There is no discernable dependence of the average bond angle or any given bond angle (e.g., C1-C2-C3) upon x.

Two recent computational investigations suggest that sp-carbon chains should be intrinsically nonlinear due to low-frequency vibrational modes of the chain.[20,28] Indeed, our DFT calculations confirm that the diplatinum compounds feature a number of low-frequency vibrations of the carbon chain, both in- and out-of-plane. The frequency of these vibrations monotonically decreases as the chain lengthens (e.g., 146 cm^{-1} in **PtC$_4$Pt** to 4 cm^{-1} in **PtC$_{26}$Pt**), which indicates progressively higher flexibility with longer chains.[19] However, a detailed investigation and analysis of these effects is outside the scope of the present work.

The shallow nature of the energy surface for chain bending was further supported by a calculation with **PtC$_{12}$Pt**. The complex $trans,trans$-[(C_6F_5)(p-tol$_3$P)$_2$Pt(C≡C)$_6$Pt(P-p-tol$_3$)$_2$-(C_6F_5)] crystallizes with the "most bent" carbon chain known to date.[11,22] The average Pt-C$_{sp}$-C$_{sp}$/C$_{sp}$-C$_{sp}$-C$_{sp}$ bond angle in this bowed structure is 174.6°. When all Pt-C$_{sp}$-C$_{sp}$ and C$_{sp}$-C$_{sp}$-C$_{sp}$ bond angles in **PtC$_{12}$Pt** were constrained to 174° in a bow conformation with C_{2v} symmetry, the increase in energy was only 2 kcalmol^{-1} relative to the unconstrained, nearly linear structure. This quantity is well within the range of crystal packing forces.

Conclusion

Computations using the model sp-carbon-chain complexes **PtC$_x$Pt** reproduce many structural and electronic features of the real systems $trans,trans$-[(X)(R$_3$P)$_2$Pt(C≡C)$_n$Pt-(PR$_3$)$_2$(X)], and allow a number of chain-length effects to be rationalized. NBO analyses show that as the chains lengthen, the platinum atoms become increasingly positively charged, and the carbon chains increasingly negatively charged. The negative charge is substantially localized on the two terminal C≡C atoms.

These data nicely account for the progressively shorter platinum–carbon bonds, and the greater lengths of the PtC≡C triple bonds as compared to neighboring C≡C linkages. In contrast, the polyynes **HC$_x$H** exhibit nearly constant carbon–hydrogen bond lengths, and the C≡C bonds lengthen monotonically as the middle of the chain is approached. Otherwise, the bond-length trends in these two classes of compounds are similar. All C−C bonds contract and C≡C bonds lengthen with increasing chain length, but marked C−C/C≡C bond alternation persists.

Backbonding from platinum could also influence the PtC≡C triple bond lengths. However, no evidence for such interactions is found by NBO population or charge decomposition analyses. Rather, the **PtC$_x$**$^-$ fragments function as simple σ/π donors. The HOMOs are best viewed as antibonding combinations of the highest occupied π orbital of the sp-carbon-chain fragment and the filled in-plane d orbital of the platinum fragment. They are strongly delocalized over the Pt/C$_x$/Pt framework, with platinum character rough-

ly proportional to the Pt/C$_x$/Pt composition (e.g., 31% for **PtC$_4$Pt**, 6% for **PtC$_{20}$Pt**). Hence, the HOMOs are predominantly chain-based at longer chain lengths (91% for **PtC$_{20}$Pt**).

In sharp contrast to the situation with **HC$_x$H**, the HOMO energies decrease with chain length. This is primarily due to the decrease in platinum and C$_1$ coefficients, which diminish the repulsive antibonding interactions. Accordingly, oxidations of real systems become thermodynamically more difficult. The LUMO energies decrease somewhat more with chain length, such that the HOMO–LUMO gaps also decrease. However, the increments become progressively smaller, such that a finite gap persists for the macromolecular limit, which corresponds to the one-dimensional polymeric carbon allotrope, carbyne.

Time-dependent DFT calculations reveal two UV-visible absorptions, both of which are π–π* transitions that originate in the carbon chain and redshift with chain length. The higher energy band simultaneously increases in intensity and acquires progressively more HOMO–LUMO character. The lower energy band decreases in intensity and has diminishing HOMO–LUMO character. Both are closely paralleled in real systems, with the former dominating in complexes with C$_8$ or longer chains. Data for the most related series, $trans,trans$-[(p-tol)(p-tol$_3$P)$_2$Pt(C≡C)$_n$Pt(P-p-tol$_3$)$_2$(p-tol)] (Table 7), predict a λ_{max} of 532 nm for the macromolecular limit, in accord with the persistent HOMO–LUMO energy gap.

The sp-carbon chains in **PtC$_x$Pt** deviate slightly from linearity, with average bond angles ranging from 179.9° (**PtC$_6$Pt**) to 179.2° (**PtC$_{12}$Pt**). The calculations identify chain-based low-frequency vibrational modes that range from 146 cm^{-1} in **PtC$_4$Pt** to 4 cm^{-1} in **PtC$_{26}$Pt**. The energy surfaces for introducing bow-shaped deformations with average bond angles of 174°, or rotating the endgroups, are very shallow. Hence, conformations are easily influenced by packing forces.

The synthesis and study of sp-carbon-chain complexes of the type L$_y$MC$_x$ML$_y$ continues to be a very active area, with emphasis shifting from now-quite-common <C$_8$ species to systems with longer bridges.[7,8,10–14] This paper has attempted to anticipate future developments by providing a comprehensive structural and electronic grammar for complexes with polyynediyl or (C≡C)$_n$ linkages of medium to long to infinite lengths. The computational results nicely rationalize the somewhat scant existing data, including phenomena that are at first glance surprising. They can be expected to extrapolate to other metal endgroups, and provide an excellent foundation for the interpretation of future experimental observations.

[1] Review of C$_x$ complexes: M. I. Bruce, P. J. Low, M. I. Bruce, *Adv. Organomet. Chem.* **2004**, *50*, 179.

[2] P. J. Kim, H. Masai, K. Sonogashira, N. Hagihara, *Inorg. Nucl. Chem. Lett.* **1970**, *6*, 181.

[3] FeC$_8$Fe complexes: a) F. Coat, C. Lapinte, *Organometallics* **1996**, *15*, 477; b) F. Coat, F. Paul, C. Lapinte, L. Toupet, K. Costuas, J.-F. Halet, *J. Organomet. Chem.* **2003**, *683*, 368.

[4] RuC$_8$Ru, MoC$_8$Mo, and WC$_8$W complexes: a) M. I. Bruce, M. Ke, P. J. Low, B. W. Skelton, A. H. White, *Organometallics* **1998**, *17*, 3539; b) M. I. Bruce, B. D. Kelly, B. W. Skelton, A. H. White, *J. Organomet. Chem.* **2000**, *604*, 150.

[5] RuC$_8$Ru complexes: a) K.-T. Wong, J.-M. Lehn, S.-M. Peng, G.-H. Lee, *Chem. Commun.* **2000**, 2259; b) G.-L. Xu, G. Zou, Y.-H. Ni, M. C. DeRosa, R. J. Crutchley, T. Ren, *J. Am. Chem. Soc.* **2003**, *125*, 10057.

[6] AuC$_8$Au complexes: W. Lu, H.-F. Xiang, N. Zhu, C.-M. Che, *Organometallics* **2002**, *21*, 2343.

[7] FeC$_8$Fe and FeC$_{12}$Fe complexes: a) M. Akita, M.-C. Chung, A. Sakurai, S. Sugimoto, M. Terada, M. Tanaka, Y. Moro-oka, *Organometallics* **1997**, *16*, 4882; b) A. Sakurai, M. Akita, Y. Moro-oka, *Organometallics* **1999**, *18*, 3241; c) M. Akita, A. Sakurai, Y. Moro-oka, *Chem. Commun.* **1999**, 101.

[8] ReC$_8$Re, ReC$_{10}$Re, ReC$_{12}$Re, ReC$_{16}$Re, and ReC$_{20}$Re complexes: R. Dembinski, T. Bartik, B. Bartik, M. Jaeger, J. A. Gladysz, *J. Am. Chem. Soc.* **2000**, *122*, 810.

[9] ReC$_8$Re complexes: a) W. E. Meyer, A. J. Amoroso, C. R. Horn, M. Jaeger, J. A. Gladysz, *Organometallics* **2001**, *20*, 1115; b) C. R. Horn, J. M. Martín-Alvarez, J. A. Gladysz, *Organometallics* **2002**, *21*, 5386; c) C. R. Horn, J. A. Gladysz, *Eur. J. Inorg. Chem.* **2003**, *9*, 2211.

[10] a) PtC$_8$Pt and PtC$_{12}$Pt complexes: T. B. Peters, J. C. Bohling, A. M. Arif, J. A. Gladysz, *Organometallics* **1999**, *18*, 3261; b) The PtC$_{10}$Pt, PtC$_{16}$Pt, and PtC$_{20}$Pt homologues of the complexes in this communication will be reported in future papers: Q. Zheng, J. A. Gladysz, Universität Erlangen-Nürnberg, unpublished data.

[11] PtC$_8$Pt, PtC$_{12}$Pt, and PtC$_{16}$Pt complexes: W. Mohr, J. Stahl, F. Hampel, J. A. Gladysz, *Chem. Eur. J.* **2003**, *9*, 3324.

[12] PtC$_8$Pt and PtC$_{12}$Pt complexes: J. Stahl, J. C. Bohling, E. B. Bauer, T. B. Peters, W. Mohr, J. M. Martín-Alvarez, F. Hampel, J. A. Gladysz, *Angew. Chem.* **2002**, *114*, 1951; *Angew. Chem. Int. Ed.* **2002**, *41*, 1871.

[13] RuC$_{12}$Ru complexes: S. Rigaut, J. Perruchon, L. Le Pichon, D. Touchard, P. H. Dixneuf, *J. Organomet. Chem.* **2003**, *670*, 37.

[14] RuC$_8$Ag and RuC$_{14}$Ru complexes: A. B. Antonova, M. I. Bruce, B. G. Ellis, M. Gaudio, P. A. Humphrey, M. Jevric, G. Melino, B. K. Nicholson, G. J. Perkins, B. W. Skelton, B. Stapleton, A. H. White, N. N. Zaitseva, *Chem. Commun.* **2004**, 960.

[15] a) R. F. Curl, *Angew. Chem.* **1997**, *109*, 1636; *Angew. Chem. Int. Ed. Engl.* **1997**, *36*, 1567; b) H. Kroto, *Angew. Chem.* **1997**, *109*, 1648; *Angew. Chem. Int. Ed. Engl.* **1997**, *36*, 1579; c) R. E. Smalley, *Angew. Chem.* **1997**, *109*, 1666; *Angew. Chem. Int. Ed. Engl.* **1997**, *36*, 1595.

[16] a) J. A. McCleverty, M. D. Ward, *Acc. Chem. Res.* **1998**, *31*, 842; b) J.-P. Launay, C. Coudret in *Electron Transfer in Chemistry, Vol. 5* (Ed.: V. Balzani), Wiley-VCH, Weinheim, Germany, **2001**, Part 1, Chapter 1; c) L. De Cola, P. Belser in *Electron Transfer in Chemistry, Vol. 5* (Ed.: V. Balzani), Wiley-VCH, Weinheim, Germany, **2001**, Part 1, Chapter 3; d) F. Scandola, C. Chiorboli, M. T. Indelli, M. A. Rampi in *Electron Transfer in Chemistry, Vol. 3* (Ed.: V. Balzani), Wiley-VCH, Weinheim, Germany, **2001**, Part 2, Chapter 3; e) R. L. Carrol, C. B. Gorman, *Angew. Chem.* **2002**, *114*, 4556; *Angew. Chem. Int. Ed.* **2002**, *41*, 4378; f) F. Paul, C. Lapinte in *Unusual Structures and Physical Properties in Organometallic Chemistry* (Eds.: M. Gielen, R. Willem, B. Wrackmeyer), Wiley, New York, **2002**, pp. 220–291.

[17] a) D. L. Lichtenberger, S. K. Renshaw, *Organometallics* **1993**, *12*, 3522; b) J. E. McGrady, T. Lovell, R. Stranger, M. G. Humphrey, *Organometallics* **1997**, *16*, 4004; c) K. D. John, T. C. Stoner, M. D. Hopkins, *Organometallics* **1997**, *16*, 4948; d) O. F. Koentjoro, R. Rousseau, P. J. Low, *Organometallics* **2001**, *20*, 4502.

[18] L. Horny, N. D. K. Petraco, C. Pak, H. F. Schaefer, III, *J. Am. Chem. Soc.* **2002**, *124*, 5861.

[19] A. Scemama, P. Chaquin, M.-C. Gazeau, Y. Bénilan, *J. Phys. Chem. A* **2002**, *106*, 3828.

[20] R. Zahradník, L. Šroubková, *Helv. Chim. Acta* **2003**, *86*, 979.

[21] Additional relevant recent experimental and computational results: a) T. Pino, H. Ding, F. Güthe, J. P. Maier, *J. Chem. Phys.* **2001**, *114*, 2208; b) U. Mölder, P. Burk, I. A. Koppel, *Int. J. Quantum Chem.* **2001**, *82*, 73; c) D. A. Kirkwood, M. Tulej, M. V. Pachkov, M. Schnaiter, F. Güthe, M. Grutter, M. Wyss, J. P. Maier, G. Fischer, *J. Chem. Phys.* **1999**, *111*, 9280; d) C. Zhang, Z. Cao, W. Haishun, Q. Zhang, *Int. J. Quantum Chem.* **2004**, *98*, 299.

[22] S. Szafert, J. A. Gladysz, *Chem. Rev.* **2003**, *103*, 4175.

[23] a) M. I. Bruce, P. J. Low, K. Costuas, J.-F. Halet, S. P. Best, G. A. Heath, *J. Am. Chem. Soc.* **2000**, *122*, 1949; b) H. Jiao, K. Costuas, J. A. Gladysz, J.-F. Halet, M. Guillemot, L. Toupet, F. Paul, C. Lapinte, *J. Am. Chem. Soc.* **2003**, *125*, 9511; c) M. I. Bruce, J.-F. Halet, B. le Guennic, B. W. Skelton, M. E. Smith, A. H. White, *Inorg. Chim. Acta* **2003**, *350*, 175.

[24] a) P. Belanzoni, N. Re, M. Rosi, A. Sgamellotti, C. Floriani, *Organometallics* **1996**, *15*, 4264; b) P. Belanzoni, N. Re, A. Sgamellotti, C. Floriani, *J. Chem. Soc. Dalton Trans.* **1997**, 4773; c) P. Belanzoni, N. Re, A. Sgamellotti, C. Floriani, *J. Chem. Soc. Dalton Trans.* **1998**, 1825; d) P. Belanzoni, A. Sgamellotti, N. Re, C. Floriani, *Inorg. Chem.* **2000**, *39*, 1147.

[25] Z. Cao, Q. Zhang, *Chem. Eur. J.* **2004**, *10*, 1920.

[26] See also: B. Bildstein, O. Loza, Y. Chizhov, *Organometallics* **2004**, *23*, 1825.

[27] a) H. Jiao, J. A. Gladysz, *New J. Chem.* **2001**, *25*, 551; b) P. Belanzoni, N. Re, A. Sgamellotti, *J. Organomet. Chem.* **2002**, *656*, 156.

[28] J. Neugebauer, M. Reiher, *J. Phys. Chem. A* **2004**, *108*, 2053.

[29] M. Springborg, R. C. Albers, *Phys. Rev. B* **1996**, *53*, 10626.

[30] *Jaguar 5.0*, Schrodinger, LLC, Portland, Oregon, **2002**.

[31] Gaussian 98 (Revision A.11), M. J. Frisch, G. W. Trucks, H. B. Schlegel, G. E. Scuseria, M. A. Robb, J. R. Cheeseman, V. G. Zakrzewski, J. A. Montgomery, Jr., R. E. Stratmann, J. C. Burant, S. Dapprich, J. M. Millam, A. D. Daniels, K. N. Kudin, M. C. Strain, O. Farkas, J. Tomasi, V. Barone, M. Cossi, R. Cammi, B. Mennucci, C. Pomelli, C. Adamo, S. Clifford, J. Ochterski, G. A. Petersson, P. Y. Ayala, Q. Cui, K. Morokuma, D. K. Malick, A. D. Rabuck, K. Raghavachari, J. B. Foresman, J. Cioslowski, J. V. Ortiz, B. B. Stefanov, G. Liu, A. Liashenko, P. Piskorz, I. Komaromi, R. Gomperts, R. L. Martin, D. J. Fox, T. Keith, M. A. Al-Laham, C. Y. Peng, A. Nanayakkara, C. Gonzalez, M. Challacombe, P. M. W. Gill, B. G. Johnson, W. Chen, M. W. Wong, J. L. Andres, M. Head-Gordon, E. S. Replogle, J. A. Pople, Gaussian, Inc., Pittsburgh, PA, **1998**.

[32] a) J. C. Slater, *Quantum Theory of Molecules and Solids, Vol. 4: The Self-Consistent Field for Molecules and Solids*, McGraw-Hill, New York, **1974**; b) A. D. Becke, *Phys. Rev. A* **1988**, *38*, 3098; c) S. H. Vosko, L. Wilk, M. Nusair, *Can. J. Phys.* **1980**, *58*, 1200; d) C. Lee, W. Yang, R. G. Parr, *Phys. Rev. B* **1988**, *37*, 785 and implemented as described by B. Miehlich, A. Savin, H. Stoll, H. Preuss, *Chem. Phys. Lett.* **1989**, *157*, 200; e) P. J. Stephens, F. J. Devlin, C. F. Chabalowski, M. J. Frisch, *J. Phys. Chem.* **1994**, *98*, 11623.

[33] P. J. Hay, W. R. Wadt, *J. Chem. Phys.* **1985**, *82*, 299.

[34] E. D. Glendening, J. K. Badenhoop, A. E. Reed, J. E. Carpenter, J. A. Bohmann, C. M. Morales, F. Weinhold, (Theoretical Chemistry Institute, University of Wisconsin, Madison, WI, 2001) *NBO 5.0*; http://www.chem.wisc.edu/~nbo5.

[35] a) The CDA methodology is described in S. Dapprich, G. Frenking, *J. Phys. Chem.* **1995**, *99*, 9352. Additional applications to transition metal systems can be found in the following references: b) R. K. Szilagyi, G. Frenking, *Organometallics* **1997**, *16*, 4807; c) C. Boehme, G. Frenking, *Chem. Eur. J.* **1999**, *5*, 2184; d) A. Beste, G. Frenking, Z. *Anorg. Allg. Chem.* **2000**, *626*, 381; e) Gudat, D. M. Nieger, K. Schmitz, L. Szarvas, *Chem. Commun.* **2002**, 1820; f) F. R. Sensato, R. Custodio, E. Longo, V. S. Safont, J. Andres, *J. Org. Chem.* **2003**, *68*, 5870.

[36] a) S. I. Gorelsky, A. B. P. Lever, *J. Organomet. Chem.* **2001**, *635*, 187; b) http://www.stanford.edu/~gorelsky/software/aomix-s/.

[37] These values are for the least-squares planes [(P$_A$–Pt$_A$–P$_A$)+Pt$_B$] and [P$_A$+(P$_B$–Pt$_B$–P$_B$)]. The inclusion of a platinum from each terminus minimizes non-idealities arising from chain curvature. When

planes defined by three or four atoms from a single endgroup are used, slightly different torsion angles are usually obtained.

[38] For the sake of internal consistency we performed our own calculations on **HC$_x$H** (x = 4, 6, 8, 10, 12, 14, 16, 18, 20, 26, 40) using the same level of theory as for **PtC$_x$Pt**, as well as one previous computational study of **HC$_x$H**.[21a] We obtained essentially the same results as found earlier, and selected data are provided in Tables s1 and s3 of the Supporting Information.

[39] For the complex *trans,trans*-[(C$_6$F$_5$)(*p*-tol$_3$P)$_2$Pt(C≡C)$_4$Pt(P-*p*-tol)$_2$(C$_6$F$_5$)],[11] the C1/C2 triple bond is unambiguously longer than the C3/C4 triple bond (1.252(6) versus 1.209(6) Å).

[40] E. J. Bylaska, J. H. Weare, R. Kawai, *Phys. Rev. B* **1998**, *58*, R7488.

[41] For recent overview of NBO see: F. Weinhold, C. Landis, *Chem. Educ.: Res. Pract. Eur.* **2001**, *2*, 91.

[42] R. Eastmond, T. R. Johnson, D. R. M. Walton, *J. Organomet. Chem.* **1973**, *50*, 87.

[43] A reviewer has suggested the possibility of a relationship between the optimized bond lengths and Pauling bond orders, as exemplified in X. Cao, W. Wu, Q. Zhang, *Int. J. Quantum Chem.* **2003**, *94*, 144. However, the excellent correlations found for hydrocarbon systems do not extrapolate to the complexes **PtC$_x$Pt**.

[44] a) Q. Fan, G. V. Pfeiffer, *Chem. Phys. Lett.* **1989**, *162*, 479; b) Q. Fan, G. V. Pfeiffer, *Chem. Phys. Lett.* **1989**, *162*, 472.

[45] I. Fleming, *Frontier Orbitals and Organic Chemical Reactions*, Wiley, New York, **1976**.

[46] This trend can also be analyzed from the standpoint of interaction diagrams (see ref. [3b] for diagrams of homologous Fe(C≡C)$_2$Fe and Fe(C≡C)$_4$Fe species). The increasing energies of the π HOMOs of the carbon-chain fragments might have been expected to give higher HOMO energies (closer match in energy to the metal fragment HOMO and enhanced filled/filled repulsive interaction). However, the progressive decrease in C1 coefficients more than offsets this effect.

[47] a) G. Schermann, T. Grösser, F. Hampel, A. Hirsch, *Chem. Eur. J.* **1997**, *3*, 1105; b) T. Gibtner, F. Hampel, J.-P. Gisselbrecht, A. Hirsch, *Chem. Eur. J.* **2002**, *8*, 408.

[48] Data for the complexes most relevant to this study, *trans,trans*-[(*p*-tol)(*p*-tol$_3$P)$_2$Pt(C≡C)$_n$Pt(P-*p*-tol$_3$)$_2$(*p*-tol)], are as follows ($E_{p,a}$ [V], CH$_2$Cl$_2$):[11b] n = 3, 0.855; n = 4, 0.971; n = 6, 1.204; n = 8, 1.264; n = 10, 1.397.

[49] a) E. J. Baerends, O. V. Gritsenko, *J. Phys. Chem. A* **1997**, *101*, 5383; b) R. Stowasser, R. Hoffmann, *J. Am. Chem. Soc.* **1999**, *121*, 3414; c) M. Bendikov, B. Solouki, N. Auner, Y. Apeloig, *Organometallics* **2002**, *21*, 1349.

[50] J. N. Louwen, R. Hengelmolen, D. M. Grove, A. Oskam, R. L. DeKock, *Organometallics* **1984**, *3*, 908.

[51] Visualized with the program Molekel: http://www.cscs.ch/molekel/.

[52] As an additional check, the effect of the CH$_2$Cl$_2$ solvent was probed by time-dependent DFT calculations using the Polarizable Continuum Model (PCM) as implemented in the Gaussian 98 suite. No significant changes in the oscillator strengths or configurations were found. These data are summarized in Table s4 of the Supporting Information.

[53] H. H. Jaffé, M. Orchin, *Theory and Applications of Ultraviolet Spectroscopy*, Wiley, New York, **1962**; Table 11.7 and accompanying discussion.

[54] Time-dependent DFT calculations on the model compound [(H$_3$P)Au(C≡C)$_n$Au(PH$_3$)] also yield transitions with characteristics similar to band II.[25a] However, in the real systems with n = 1–4 prepared to date, the bands are masked for n = 1–3.[6] Time-dependent DFT calculations on **HC$_x$H** have also been very recently reported.[21d]